Received 00th January 20xx,
Accepted 00th January 20xx

DOI: 10.1039/x0xx00000x

www.rsc.org/

Identification and Characterisation of High Energy Density P2-Type $Na_{2/3}[Ni_{1/3-y/2}Mn_{2/3-y/2}Fe_y]O_2$ Compounds for Na-ion Batteries

J. W. Somerville,[a] N. Tapia-Ruiz,[a,c] A. Sobkowiak,[a] R. House,[a] S. Ramos,[b] A. V. Chadwick,[b] M. Roberts,[a] U. Maitra,[a] and P. G. Bruce[a]

The composition space between MnO_2, $NaFeO_2$, and $Na[Ni_{1/2}Mn_{1/2}]O_2$ has been explored with the goal of identifying Earth-abundant single-phase P2 cathode materials. This has led to the identification of two compounds, P2 $Na_{2/3}[Ni_{1/3-y/2}Mn_{2/3-y/2}Fe_y]O_2$ (y = 1/6, 1/3) which exhibit state of the art specific energies. These materials were further evaluated through galvanostatic cycling and x-ray absorption spectroscopy.

Introduction

Na-ion batteries could one day find a niche in replacing Li-ion batteries for certain applications (such as grid storage) because of the greater elemental abundance of Na leading to reduced costs.[1] However, while cathode and anode chemistries exist, there remains a need for better materials.[2] This work focuses on the discovery of new cathode materials.

Among potential candidates, Na layered transition metal oxides ($NaMO_2$, M = Mn, Fe, Co, Ni, etc.) have the benefit of high energy densities.[3] They crystallise into various structural polymorphs including P2, O3, and P3 where P and O indicate the Na site type (P: Trigonal Prismatic, O: Octahedral) and the number indicates the stacking sequence (eg. P2: ABBA).[4] The P2 structure is generally considered optimal due to its greater Na mobility in prismatic sites. [5]

One of the prime candidates among $NaMO_2$'s is P2 - $Na_{2/3}[Mn_{1/2}Fe_{1/2}]O_2$ because it contains low cost, Earth-abundant transition metals and has a high reversible capacity of 190 mAh g^{-1} as summarized in Table 1.[6] The charge compensation in this material is achieved by utilising $Mn^{3+/4+}$ (low voltage) and $Fe^{3+/4+}$ (high voltage) redox couples (as per Equation 1).[7] This results in a moderate average discharge voltage of 2.75 V vs. Na/Na^+ and overall specific energy of 523 Wh kg^{-1}.[6]

(1) $Na^+_{2/3}[Mn^{3.67+}_{1/2}Fe^{3+}_{1/2}]O^{2-}_2 \rightarrow [Mn^{4+}_{1/2}Fe^{4+}_{1/2}]O^{2-}_2$

Another P2-type compound, $Na_{2/3}[Ni_{1/3}Mn_{2/3}]O_2$, has been observed to have a high voltage and specific energy.[8] When this material is cycled in the 1.5-4.5 V vs. Na/Na^+ range, it displayed a capacity of 210 mAh g^{-1} and an average discharge voltage of 3.01 V vs. Na/Na^+. This, indeed corresponds to a higher specific energy of 638 Wh kg^{-1} as complete Na extraction (2/3 mol Na per formula unit) can be theoretically compensated by the high voltage $Ni^{2+/4+}$ redox couple (as per Equation 2).

(2) $Na^+_{2/3}[Ni^{2+}_{1/3}Mn^{4+}_{2/3}]O^{2-}_2 \rightarrow [Ni^{4+}_{1/3}Mn^{4+}_{2/3}]O^{2-}_2$

However, this compound suffers from poor cycling stability. The goal of this work was to search for a compound within the MnO_2, $NaFeO_2$ and $Na[Ni_{1/2}Mn_{1/2}]O_2$ composition space with a P2 structure and which has predominate charge compensation through the high voltage Fe and Ni redox couples (to achieve similar specific energies as $Na_{2/3}[Ni_{1/3}Mn_{2/3}]O_2$) and reduced capacity fading by suppressing the transition to the O2 structure on charging (similar to $Na_{2/3}[Mn_{1/2}Fe_{1/2}]O_2$)[6]. This resulted in the identification and further analysis of two new materials based on P2 - $Na_{2/3}[Ni_{1/3-y/2}Mn_{2/3-y/2}]Fe_yO_2$ where y = 1/6 and 1/3. We show that P2 - $Na_{2/3}[Ni_{1/4}Mn_{7/12}Fe_{1/6}]O_2$ can deliver 598 Wh kg^{-1}, 14% higher than that of previously studied P2 - $Na_{2/3}[Fe_{1/2}Mn_{1/2}]O_2$. Furthermore, the more Fe-rich compound, $Na_{2/3}[Ni_{1/6}Mn_{1/2}Fe_{1/3}]O_2$ retains 67% of its original capacity after 50 cycles, improved significantly over Fe-free $Na_{2/3}[Ni_{1/3}Mn_{2/3}]O_2$, which retains only 38%. X-ray absorption spectroscopy revealed that Ni is oxidized to partially compensate the initial Na extraction on the first charge, whereas changes on the Fe edge indicate that Fe also likely plays a role. Mn is reduced when

Table 1. A comparison of electrochemical performance data for previously reported $Na_{2/3}[Mn_{1/2}Fe_{1/2}]O_2$ and the cathode materials first reported here (shown in bold). *$Na_{2/3}[Mn_{1/2}Fe_{1/2}]O_2$ was reported to be cycled in the 1.5 – 4.2 V vs. Na/Na^+ range[6] whereas the bolded compounds, reported here, were cycled in the 1.5 - 4.5 V range.

TM Composition	*1st Dis. Cap (mAhg^{-1})*	*1st Cycle Avg. Dis. Voltage*	*1st Spec. Energy (Whkg^{-1})*	*50 Cycle Dis. Cap. Retention*
$Na_{2/3}$ $[Mn_{1/2}Fe_{1/2}]$ O_2*	190	2.75	523	65%
$Na_{2/3}[Ni_{1/3}Mn_{2/3}]O_2$	**212**	**3.01**	**638**	**38%**
$Na_{2/3}[Ni_{1/4}Mn_{7/12}Fe_{1/6}]O_2$	**202**	**2.96**	**598**	**61%**
$Na_{2/3}[Ni_{1/6}Mn_{1/2}Fe_{1/3}]$ O_2	**201**	**2.91**	**585**	**67%**

[a] Depts. of Materials and Chemistry, University of Oxford, Parks Rd, Oxford, UK
[b] School of Physical Sciences, University of Kent, Canterbury, Kent, UK
† Footnotes relating to the title and/or authors should appear here.
Electronic Supplementary Information (ESI) available: [details of any supplementary information available should be included here]. See DOI: 10.1039/x0xx00000x

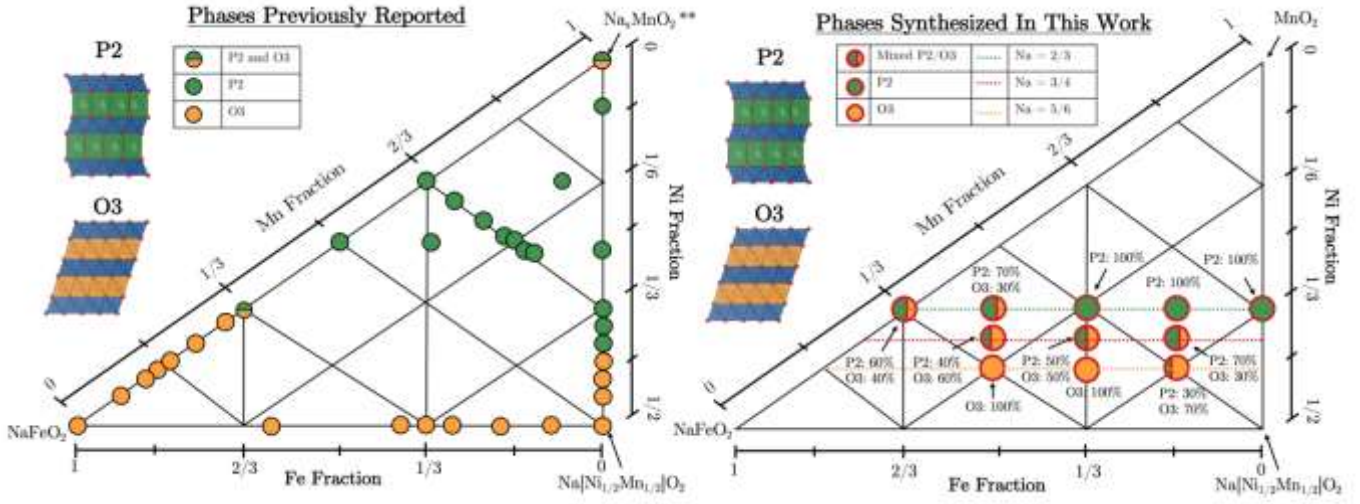

Figure 1 Two ternary phase-composition diagrams between the end-members $NaFeO_2$, $Na[Ni_{1/2}Mn_{1/2}]O_2$, and MnO_2 (** Previously reported materials are often synthesized with varying Na contents, hence the end member Na_xMnO_2, $0 \le x \le 1$). Circles represent compounds either reported in literature (left diagram) or synthesized in this work (right diagram). The green-filled circles indicate the P2 structure, the orange-filled circles indicate the O3 structure, and the circles with both colours represent mixed phases (vertically divided) or that both phases are possible to obtain by varying the synthesis conditions and Na content (horizontally divided). See Figure S1, Supporting Information, for XRD patterns of the in-house prepared compositions.

the material is electrochemically discharged to Na contents greater than that of the pristine compound, giving extra capacity at voltages below 2.5 V vs Na/Na^+. All relevant experimental methods are described in the Supporting Information

Results

Ternary Phase-Composition Diagram

Figure 1 shows two ternary phase-composition diagrams between the end members $Na[Ni_{1/2}Mn_{1/2}]O_2$, $NaFeO_2$, and MnO_2. The diagram on the left summarizes relevant compositions from the literature[7,9–19] whereas the diagram on the right reports the compounds investigated here. It was immediately evident from plotting these previously reported compositions that P2 compounds (green filled circles) tended to be more Mn-rich (and generally less Na) whereas O3-type compounds (orange filled circles) tended to be more Ni- and Fe-rich (and generally more Na). However, the mid-to-lower section of the diagram is not well explored although it is this region where there is an opportunity to synthesise P2 compounds which maximise the amount of Ni and Fe (high voltage redox couples). Efforts were therefore focussed on this space.

In total, eleven compositions were synthesised in and around this unexplored region. Phase identification and sample purity were determined for each from refinement of x-ray diffraction patterns (shown in SI).

We observe a clear trend in the preference for forming the O3-type rather than the P2-type structure as the composition becomes more Na-rich (towards $NaFeO_2$ and $Na[Ni_{1/2}Mn_{1/2}]O_2$), in agreement with previous reports.[7] However, a correlation between Fe content and phase purity can also be seen. For example, moving across the composition series $Na_{3/4}[Ni_{3/8-y/2}Mn_{5/8-y/2}Fe_y]O_2$ where $1/6 \le y \le 1/2$ (red dashed line in Figure 1), the phase fraction of the O3 structure increased from 30% at $y = 1/6$, to as much as 60% at $y = 1/2$. The trend toward the O3 structure with increased Fe content is maintained for the higher and lower composition series in the diagram corresponding to Na contents of 2/3 and 5/6, $Na_{2/3}[Ni_{1/3-y/2}Mn_{2/3-y/2}Fe_y]O_2$ and $Na_{5/6}[Ni_{5/12-y/2}Mn_{7/12-y/2}Fe_y]O_2$, respectively (green and yellow dashed lines). No evidence of compositional segregation was observed as shown in Figure S2.

In addition to these useful trends, we were able to identify two compounds, $Na_{2/3}[Ni_{1/4}Mn_{7/12}Fe_{1/6}]O_2$ and $Na_{2/3}[Ni_{1/6}Mn_{1/2}Fe_{1/3}]O_2$, which maintained the P2 structure despite relatively high Ni and Fe content. It is worth noting that even though these compositions were synthesised with 2/3 mol Na per formula unit, the number of available Na sites still theoretically allows for 1 mol Na to be cycled if extra Na is available from elsewhere in the system (sacrificial salt, excess Na in anode, etc.). These compositions were validated by ICP-MS (Table S1) and SEM showed that both samples have a similar morphology of faceted secondary particles made up of stacked layers ranging in size from 1-5 µm (Figure S3). Some crystallographic changes were observed when the powders came in contact with water (Figure S4) and therefore, the samples were prepared and processed in an argon glovebox.

Electrochemical Performance

$Na_{2/3}[Ni_{1/4}Mn_{7/12}Fe_{1/6}]O_2$ and $Na_{2/3}[Ni_{1/6}Mn_{1/2}Fe_{1/3}]O_2$ were cycled galvanostatically between 1.5 and 4.5 V (vs. Na+/Na) along with the Fe-free compound, $Na_{2/3}[Ni_{1/3}Mn_{2/3}]O_2$, as a point of reference. Figure 2a-c shows the electrochemical load curves of these three compositions. A summary of the subsequently discussed performance values is presented in Table 1. An increasing Fe content along the $Na_{2/3}[Ni_{1/3-y/2}Mn_{2/3-y/2}Fe_y]O_2$ series ($y = 0, 1/6, 1/3$) was found to result in a slight decrease of the discharge capacities during the first cycle, from 212 mAh g^{-1} for $y = 0$, to 202 mAh g^{-1} for $y = 1/6$ and 201 mAh g^{-}

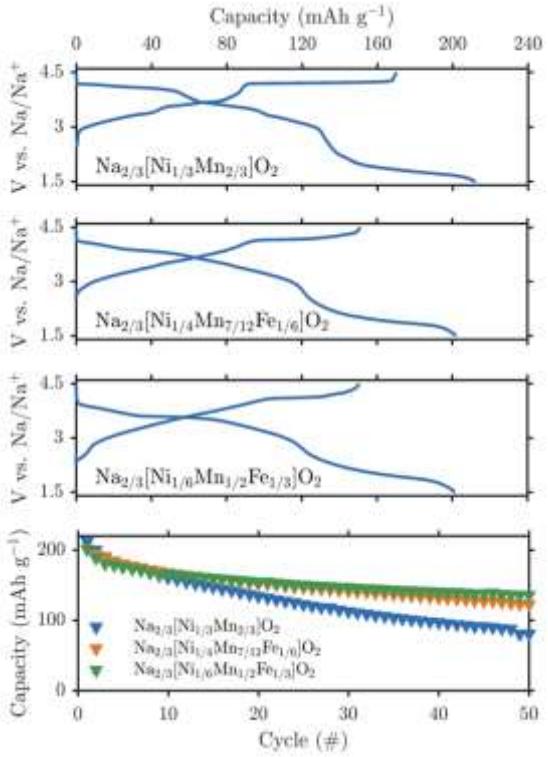

Figure 2 . The first charge and discharge load curves are shown for $Na_{2/3}[Ni_{1/3-y/2}Mn_{2/3-y/2}Fe_y]O_2$ where a) y = 0, b) y = 1/6 and c) y = 1/3. Each compound's discharge capacity retention is shown in d).

[1] for the y = 1/3. Nevertheless, given the relatively high average discharge voltages (3.01 V for y = 0, 2.96 V for y = 1/6 and 2.91 V for y = 1/3), the observed capacities for all three compositions correspond to high specific energies of 640, 599, and 587 Wh kg^{-1}, respectively, which are among the best reported for Na-ion insertion compounds.[20] Moreover, while a lower Ni-content makes the material more environment friendly, the increase in Fe content was also found to significantly improve the capacity retention (shown in Figure 2d) during prolonged cycling where the y = 1/3 sample maintained a discharge capacity of almost 136 mAh g^{-1} (67% of the initial capacity) after 50 cycles, while the corresponding value for the Fe-free sample, y = 0, was 81 mAh g^{-1} (38% of the initial capacity). The rather low capacity retention of the Fe-free sample is not unexpected as capacity retention does tend to decrease for compounds charged to high states of deintercalation (low Na contents). A potential explanation for the improved capacity retention for the Fe-containing samples is a difference in the high voltage phase transition mechanism, as seen in Figure S5. Further work is currently being carried out to better understand the capacity degradation mechanism and will be reported separately. In order to understand the charge compensation mechanism on Na extraction and re-insertion, x-ray absorption spectroscopy was carried out at each of the transition metal K-edges.

X-Ray Absorption Spectroscopy

XANES spectra for Mn, Ni, and Fe were collected from samples extracted from cells stopped at key points (shown in Figure S7) during the first charge/discharge cycle.

As a reference for the below description of the XANES spectra the charge compensation anticipated from the electrochemistry can be summarised in the following equations (assuming Ni is oxidized before Fe)[21]:

(3) $Na^+_{2/3}[Ni^{2+}_{1/4}Mn^{4+}_{7/12}Fe^{3+}_{1/6}]O^{2-}_2$
$\rightarrow Na^+_{0.1}[Ni^{4+}_{1/4}Mn^{4+}_{7/12}Fe^{3.4+}_{1/6}]O^{2-}_2$

(4) $Na^+_{2/3}[Ni^{2+}_{1/6}Mn^{4+}_{1/2}Fe^{3+}_{1/3}]O^{2-}_2$
$\rightarrow Na^+_{0.1}[Ni^{4+}_{1/6}Mn^{4+}_{1/2}Fe^{3.7+}_{1/6}]O^{2-}_2$

The oxidation states for Mn, Fe, and Ni in the pristine compounds, y = 1/6 and y = 1/3, were confirmed to be 4+, 3+, and 2+, respectively, by comparing the absorption edge energies to standards.

The shift of the Mn K-edge (Figure 3a, 3g) in both compositions was negligible during the initial charge process consistent with Equations 3 and 4 where Mn remains 4+ at the end of charge. Only when discharged below 2.5 V vs. Na/Na$^+$ does a significant negative shift become visible (Figure 3d, 3j). This shift towards lower energies indicates the reduction of Mn^{4+} toward Mn^{3+}, which is fully expected when the material is sodiated beyond the pristine Na content of 2/3 mol per formula unit.

As in other $NaMO_2$ materials, the Fe K-edge for both the y = 1/6 and the y = 1/3 compositions (Figure 3b, 3h) show no significant movement of the absorption edges throughout the charge cycle, therefore exact quantification is difficult. Definite changes to the peak shape are observed, however, which is consistent with previous observations during Fe oxidation of $Na_{2/3}[Fe_{1/2}Mn_{1/2}]O_2$.[6] There are much greater peak shape changes for the y = 1/3 composition compared to y = 1/6 on charge, which follows the anticipated Fe oxidation state changes of Equation 3 and 4. The pre-edge also increases slightly in intensity for the samples at 4.2 and 4.5 V vs Na/Na$^+$. This increase in the pre-edge absorption could be due to the new hole-states created in the Fe 3d states and/or an increased distortion around the Fe octahedra.[23] On discharge, this pre-edge intensity and the edge shape become identical to that of the pristine (Figure 3e, 3k).

The Ni K-edge does shift towards higher energies on charge for both samples (Figure 3c, 3i). For the y = 1/6 composition, this movement occurs somewhat linearly with state of charge demonstrating that the Ni contributes to the charge compensation at all voltages throughout the first charge This is in clear contrast to the y = 1/3 composition which shows a dramatic shift from pristine to 4 V and only a small shift upon further charge. This is likely due to the lower amount of Ni in the y = 1/3 compound, hence it is oxidized first whereas for the y = 1/6 compound, Ni continues to be oxidized above 4 V. On discharge, the Ni edge returns to that of the pristine sample by 2.5 V vs Na/Na$^+$ with no further change on continued discharge.

Conclusions

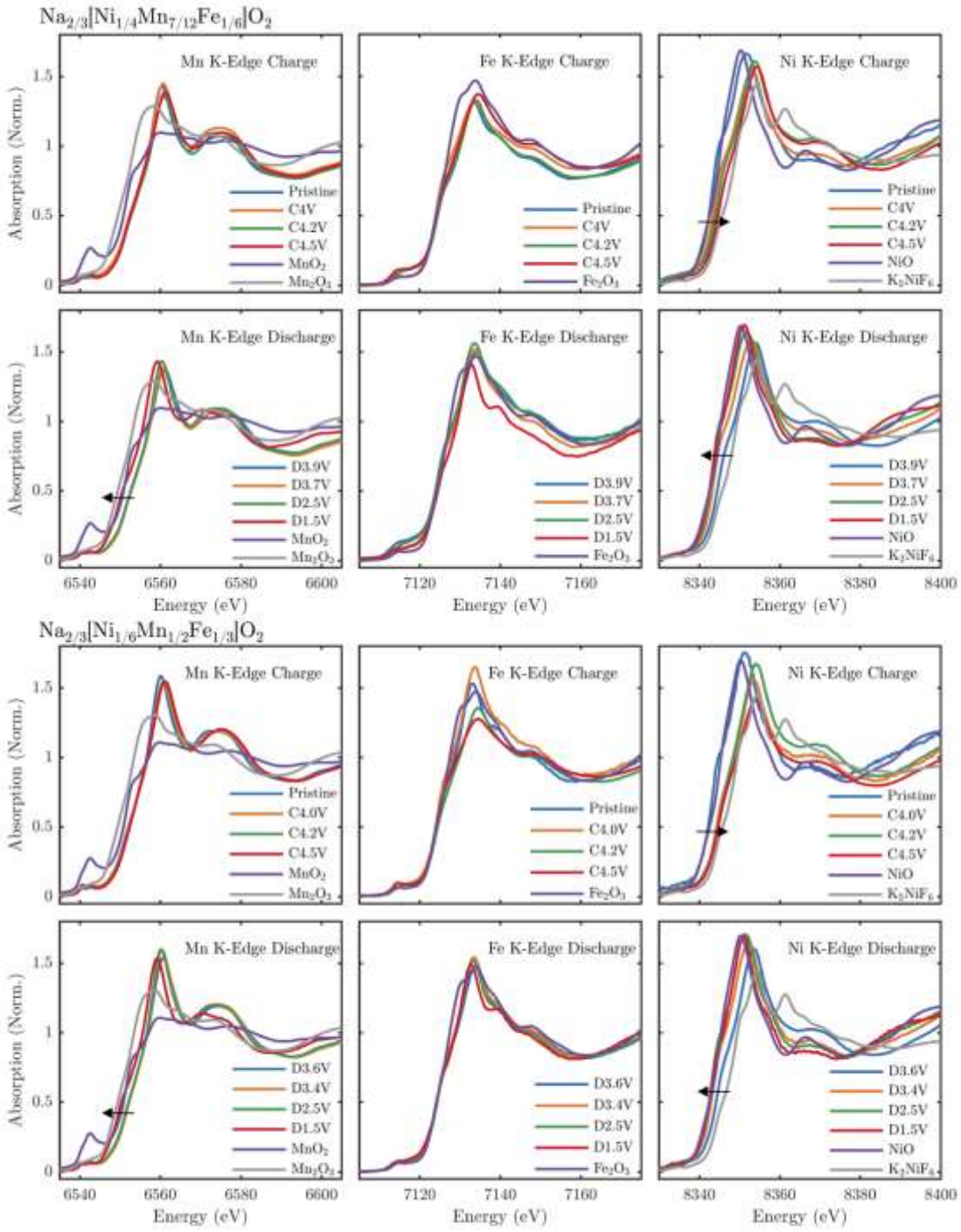

Figure 3 XANES spectra are shown for $Na_{2/3}[Ni_{1/3-y/2}Mn_{2/3-y/2}Fe_y]O_2$, a-f) y = 1/6, g-l) y = 1/3. For each compound, the K-edge absorption is shown for Mn, Fe and Ni from left to right and further separated based on where the cell was stopped during charge or discharge. Relevant standards are included in all spectra plots.

In summary, the composition space between $Na[Ni_{1/2}Mn_{1/2}]O_2$, $NaFeO_2$, and MnO_2 has been explored and P2-$Na_{2/3}[Ni_{1/4}Mn_{7/12}Fe_{1/6}]O_2$ and $Na_{2/3}[Ni_{1/6}Mn_{1/2}Fe_{1/3}]O_2$ identified as compositions that balance high energy density, cycling stability and Earth abundance. An in-depth study of the ternary phase-composition diagram has identified a correlation between the presence of Fe and favoured O3 phase formation relative to P2 at the same Na content, a relation not recognized until now. Galvanostatic cycling of these new compounds confirmed the excellent specific energies and showed that increasing Fe content improves the capacity retention. XANES measurements indicated that Ni is oxidised on the first charge, and Fe likely also plays a role in this charge compensation, although alternate characterization methods must be undertaken to verify this. On discharge, the Ni and Fe absorption edges both become identical to that of the pristine, whereas Mn shifts to lower energies demonstrating reduction to provide extra capacity below 2.5 V vs Na/Na^+. On a broader

scope, this study highlights the appealing prospect of P2-type compounds composed of Earth-abundant elements as Na-ion battery cathodes and the improvements in specific energy and capacity retention that can be achieved by tuning the transition metal composition. Further work is underway to understand the source of the improved cycling stability.

Conflicts of interest

There are no conflicts to declare.

References

1 N. Yabuuchi, K. Kubota, M. Dahbi and S. Komaba, *Chem. Rev.*, 2014, **114**, 11636–82.

2 K. Kubota and S. Komaba, *J. Electrochem. Soc.*, 2015, **162**, A2538–A2550.

3 D. Kundu, E. Talaie, V. Duffort and L. F. Nazar, *Angew. Chemie Int. Ed.*, 2015, **54**, 3431–3448.

4 C. Delmas, C. Fouassier and P. Hagenmuller, *Phys. B+C*, 1980, **99**, 81–85.

5 Y. Mo, S. P. Ong and G. Ceder, *Chem. Mater.*, 2014, **26**, 5208–5214.

6 N. Yabuuchi, M. Kajiyama, J. Iwatate, H. Nishikawa, S. Hitomi, R. Okuyama, R. Usui, Y. Yamada and S. Komaba, *Nat. Mater.*, 2012.

7 B. Mortemard de Boisse, D. Carlier, M. Guignard and C. Delmas, *J. Electrochem. Soc.*, 2013, **160**, A569–A574.

8 H. Yoshida, N. Yabuuchi, K. Kubota, I. Ikeuchi, A. Garsuch, M. Schulz-Dobrick and S. Komaba, *Chem. Commun. (Camb).*, 2014, **50**, 3677–80.

9 J. Zhao, L. Zhao, N. Dimov, S. Okada and T. Nishida, *J. Electrochem. Soc.*, 2013, **160**, A3077–A3081.

10 N. Yabuuchi, M. Yano, H. Yoshida, S. Kuze and S. Komaba, *J. Electrochem. Soc.*, 2013, **160**, A3131–A3137.

11 S. Komaba, T. Nakayama, A. Ogata, T. Shimizu, C. Takei, S. Takada, A. Hokura and I. Nakai, in *ECS Transactions*, ECS, 2009, vol. 16, pp. 43–55.

12 E. Talaie, V. Duffort, H. L. Smith, B. Fultz and L. F. Nazar, *Energy Environ. Sci.*, 2015, **8**, 2512–2523.

13 D. D. Yuan, Y. X. Wang, Y. L. Cao, X. P. Ai and H. X. Yang, *ACS Appl. Mater. Interfaces*, 2015, **7**, 8585–8591.

14 D. Yuan, X. Hu, J. Qian, F. Pei, F. Wu, R. Mao, X. Ai, H. Yang and Y. Cao, *Electrochim. Acta*, 2014, **116**, 300–305.

15 J. Cabana, N. A. Chernova, J. Xiao, M. Roppolo, K. A. Aldi, M. S. Whittingham and C. P. Grey, *Inorg. Chem.*, 2013, **52**, 8540–8550.

16 I. Hasa, D. Buchholz, S. Passerini and J. Hassoun, *ACS Appl. Mater. Interfaces*, 2015, **7**, 5206–5212.

17 R. Fielden and M. N. Obrovac, *J. Electrochem. Soc.*, 2015, **162**, A453–A459.

18 a. Mendiboure, C. Delmas and P. Hagenmuller, *J. Solid State Chem.*, 1985, **57**, 323–331.

19 W. Zhao, H. Kirie, A. Tanaka, M. Unno, S. Yamamoto and H. Noguchi, *Mater. Lett.*, 2014, **135**, 131–134.

20 H. Liu, J. Xu, C. Ma and Y. S. Meng, *Chem. Commun.*, 2015, **51**, 4693–4696.

21 Y. Nanba, T. Iwao, B. M. de Boisse, W. Zhao, E. Hosono, D. Asakura, H. Niwa, H. Kiuchi, J. Miyawaki, Y. Harada, M. Okubo and A. Yamada, *Chem. Mater.*, 2016, **28**, 1058–1065.

22 X. Wang, G. Liu, T. Iwao, M. Okubo and A. Yamada, *J. Phys. Chem. C*, 2014, **118**, 2970–2976.

23 K. Kubota, T. Asari, H. Yoshida, N. Yaabuuchi, H. Shiiba, M. Nakayama and S. Komaba, *Adv. Funct. Mater.*, 2016, **26**, 6047–6059.